RESEARCH ARTICLE

The life cycle of small- to medium-sized icebergs in the Amundsen Sea Embayment

Aleksandra K. Mazur[1,2], Anna K. Wåhlin[1] & Ola Kalén[3]

[1]Department of Marine Sciences, University of Gothenburg, Göteborg, Sweden;
[2]Institute of Oceanography, University of Gdańsk, Gdynia, Poland;
[3]Swedish Meteorological and Hydrological Institute, Göteborg, Sweden

Abstract

An object-based method for automatic iceberg detection has been applied to Advanced Synthetic Aperture Radar images in the Amundsen Sea Embayment (ASE), Antarctica. The images were acquired between 1 January 2006 and 8 April 2012 under varying meteorological, oceanographic and sea-ice conditions. During this time period, the icebergs were counted (average 1370 ± 50) and their surface area was estimated (average 1537.5 km^2). The average surface area was about 2.5 times larger than the annual calved area (620 km^2), indicating that the average iceberg age in the ASE is about 2.5 years, which was confirmed by observed residence times based on drift tracks. Most of the ASE icebergs were less than 1500 m long, and almost 90% of them were smaller than 2 km^2. The proportion of small- and medium-sized icebergs (84.4%) was significantly higher than in the open ocean, where large icebergs (>10 km^2) account for nearly the whole iceberg surface area. The opposite was true for the freshly calved icebergs in the ASE. The data indicate that the creation of icebergs in the ASE is dominated by steady small- to medium-scale calving from ice shelves fringing the embayment. In addition, rare calving events of giant icebergs occur on a decadal timescale. There is also some import of icebergs from the Bellingshausen Sea further east along the coast, in particular after large calving events there.

Keywords

Satellite radar data; object-based image analysis; iceberg size distribution; iceberg annual variations

Correspondence

Aleksandra K. Mazur, Department of Marine Sciences, University of Gothenburg, P.O. Box 461, SE-405 30 Göteborg, Sweden.
E-mail: akmazur@marine.gu.se

Abbreviations

AMSR-E: Advanced Microwave Scanning Radiometer–Earth Observing System (satellite-based instrument); AMSR2: Advanced Microwave Scanning Radiometer 2 (satellite-based instrument); ASAR: Advanced Synthetic Aperture Radar (satellite-based instrument); ASE: Amundsen Sea Embayment; Envisat: Environmental Satellite (Earth-observing satellite); ERA-Interim: European Centre for Medium-Range Weather Forecast Interim Re-analysis data set; IBCSO: International Bathymetric Chart of the Southern Ocean; NIC: US National Ice Center; SSMIS: Special Sensor Microwave Imager/Sounder (satellite-based instrument); WMO: World Meteorological Organization

Introduction

Icebergs are an important part of the hydrological cycle in the seas surrounding the Antarctic continent. They influence the local water circulation (Biddle et al. 2015; Stern et al. 2015) and primary production (e.g., Smith et al. 2007; Raiswell et al. 2008; Lancelot et al. 2009; Biddle et al. 2015; Barnes 2017). They can also have significant impact on sea-ice formation: through iceberg melt large quantities of freshwater are released into the near-surface layer, which is a key component of sea-ice formation (Björk et al. 2002; Bintanja et al. 2015). The freshwater intrusions and the cooling effect of icebergs also often facilitate sea-ice formation, creating a mixture of icebergs and sea ice (Jongma et al. 2009). Despite having significant influence on the environment and accounting for a major part of the loss of the West Antarctic Ice Sheet, icebergs are still poorly quantified. This is particularly true in the ASE (Fig. 1), the coastal area where the most rapidly melting glaciers are terminating and a region that is known for the large abundance of icebergs. The West Antarctic Ice Sheet alone contains 3.8 million km^3 of ice (Fretwell et al. 2013). If this volume of ice moved into the ocean, or melted, it would result in a global sea-level rise of about 3.3–4.3 m (Bamber et al. 2009; Fretwell et al. 2013). The average ice mass loss from glaciers into the ASE has been estimated to 670 Gt yr^{-1}, about 50% of the Antarctic ice loss (Depoorter et al. 2013;

Citation: *Polar Research* 2019, *38*, 3313, http://dx.doi.org/10.33265/polar.v38.3313

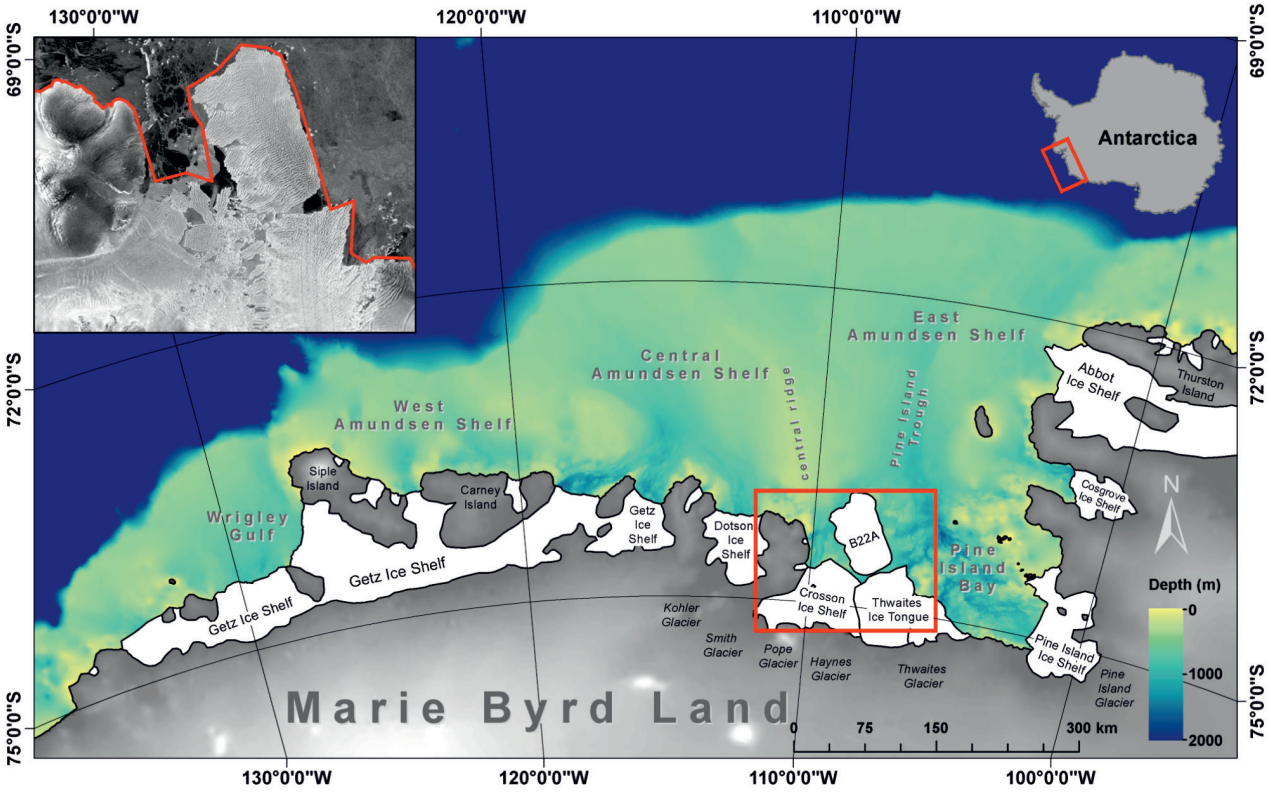

Fig. 1 Location and bathymetry of the ASE. The bathymetry is acquired from the IBCSO database (Arndt et al. 2013). An example radar image with the area excluded from the present analysis is presented in upper left.

Rignot et al. 2013). Two-thirds of this ice loss is due to calving, while one-third is due to basal melt of the ice shelves. Given that iceberg calving is such an important mechanism by which ice is moving from the continent, surprisingly little is known about their fate after calving.

Icebergs form either through calving at the floating ice shelf fronts or by disintegration of larger icebergs. Once formed, they can float away until they melt or become stranded on topographic features. These processes occur in the ASE. However, limitations in sample size and methodology in previous studies have prevented these processes from being quantified. The origin of the ASE icebergs has not been determined nor has their movement and residence time while in the embayment. It is apparent from ASAR images that a large portion of icebergs are stranded on shallow ridges (Mazur et al. 2017), but it is not known how long they stay stranded or how fast they leave the area when they become afloat. This information is of importance in modelling sea-ice, freshwater distribution and iceberg dynamics. Previous observational studies of icebergs are confined to open ocean (Tournadre et al. 2008; Tournadre et al. 2012; Tournadre et al. 2015), to small sample sizes (e.g., Romanov et al. 2012) or to a study period that is too short to perform statistical analyses of the life cycle of the icebergs (Wesche & Dierking 2015).

The objective of this work is to study, for the first time, the life cycle of icebergs in the ASE, from their origin until they leave the area. We use six years of ASAR images to estimate the input of icebergs from local ice shelves, and observe the changes of surface area, number and size distribution of icebergs during this period. Meteorological and sea-ice data are used to explain the observed changes and discuss the factors that control the iceberg residence time in the ASE. Because of the resolution limitation we focus our analyses on icebergs with surface area larger than 0.3 km^2. A few giant icebergs were observed, and the influence of these on the distribution of the smaller icebergs in the region as they break up is discussed.

We are utilizing Envisat ASAR radar data from 2006 to 2012 and the (object-based) identification technique described by Mazur et al. (2017), which allows identification of small icebergs and in all seasons. We are also using data concerning large icebergs—longer than 10 nautical miles (18.5 km)—from the NIC going back to 1978 (http://www.scp.byu.edu/data/iceberg/).

Citation: *Polar Research* 2019, *38*, 3313, http://dx.doi.org/10.33265/polar.v38.3313

Data and methods

Satellite radar data

In this study, 2445 Envisat ASAR Wide Swath Mode images (level 1b), recorded between 1 January 2006 and 8 April 2012, were analysed. Every year between 241 and 636 images were analysed (Table 1). The time step between iceberg observations depends on the revisit frequency of the Envisat satellite. It decreased from approximately nine days in 2006–09 to about two days in 2010–12. The images were acquired at C-band (5.3 GHz) and HH polarization using the ScanSAR technique (ESA 2007). The spatial resolution of the data was 150 m × 150 m and the incidence angle varied between 17 and 43°. The images were georectified to Lambert Azimuthal Equal Area projection using NEST DAT 5.1 (ESA 2015) and the subset longitude 100–135°W and latitude 70–76°S was extracted and calibrated as described by Mazur et al. (2017): radiometric distortions caused by the varying incidence angle were removed using the normalized gamma nought coefficient (γ) according to Rosich & Meadows (2004), and speckles were removed using an adaptive Frost filter (Frost et al. 1982) with a kernel size of 3×3. After filtering, the data were converted to logarithmical scale (dB).

Table 1 Number of images available and analysed in different years.

Year	Number of analysed images
2006	247
2007	346
2008	242
2009	241
2010	571
2011	636
2012	162
Total	2445

Air temperature and wind speed

The air temperature and wind data were obtained from of a global climate reanalysis data set: the ERA-Interim (Dee et al. 2011). The data set has global spatial coverage from 1979 to date and is updated in nearreal time. ERA-Interim shows the most reliable results when compared with in situ observations at the stations around Antarctica (Bracegirdle & Marshall 2012) as well as with buoys in the Bellingshausen Sea (Bracegirdle 2013). In the present study, daily averages of 2 m temperature and 10 m u and v wind components for a grid size of 1° × 1° covering the Amundsen Sea between 1 January 2006 and 8 April 2012 were used.

The average air temperature in the Amundsen Sea during the study period was −10.1°C and values below 0°C were observed for most of the year. However, positive values were noted, mostly in the northern part, at the turn of December and January (Fig. 2). The average wind speed was 7.5 m s^{-1}, but it varied significantly during the year. There was a clear seasonal variation of the wind speed, with the highest values observed during the austral winter (June–August) and the lowest during the austral summer (December–February) (Fig. 3).

Sea-ice concentration and drift data

The sea-ice concentration data were daily, 6.25 × 6.25 km resolution products, provided by the University

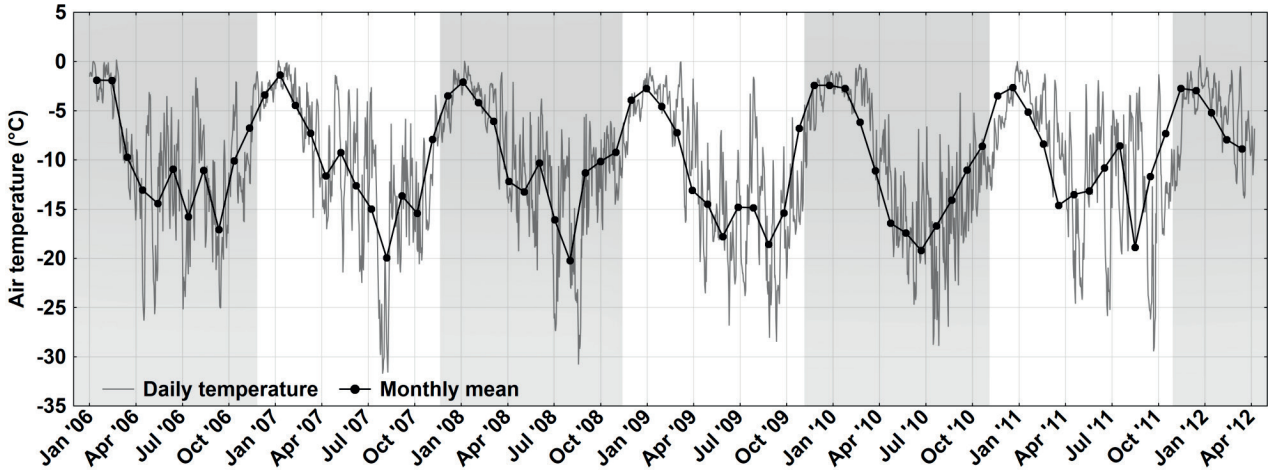

Fig. 2 Averaged daily and monthly air temperature in the ASE from ERA-Interim between 1 January 2006 and 8 April 2012 (Dee et al. 2011). Grey rectangles separate 12-month periods starting on 1 December and ending the following calendar year on 30 November.

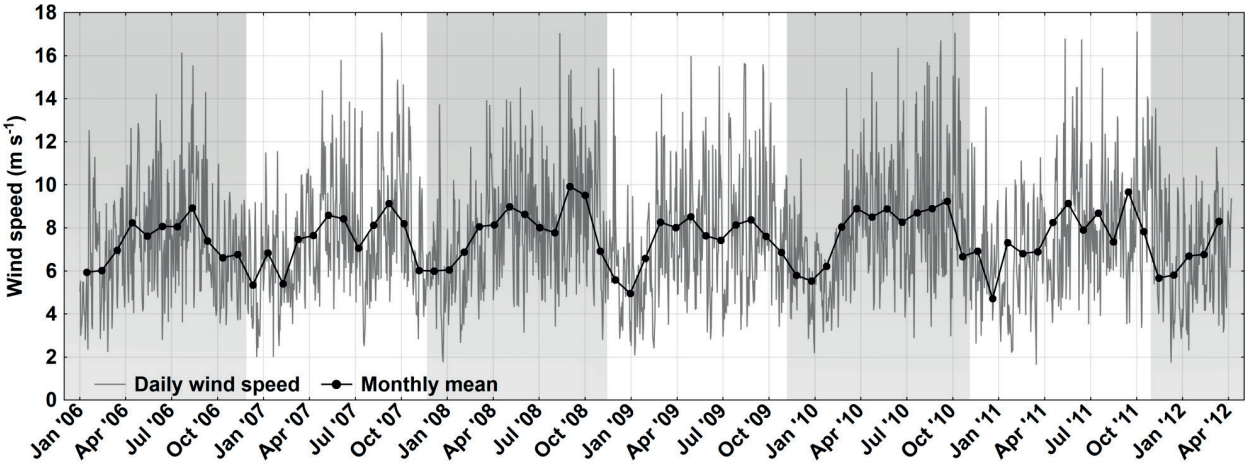

Fig. 3 Averaged daily and monthly wind speed in the ASE from ERA-Interim between 1 January 2006 and 8 April 2012 (Dee et al. 2011). Grey rectangles separate 12-month periods starting on 1 December and ending the following calendar year on 30 November.

of Bremen between 1 January 2006 and 8 April 2012 (https://seaice.uni-bremen.de). The sea-ice concentration was computed by applying the ARTIST Sea Ice algorithm to brightness temperatures measured with the 89 GHz AMSR-E channels (Spreen et al. 2008). AMSR-E was a 12-channel, six frequency, passive-microwave radiometer system, which measured horizontally and vertically polarized brightness temperatures. It was launched on 2 May 2002 and operated until 4 October 2011.

As the AMSR-E stopped working in October 2011 and the next instrument (AMSR2) has provided data since 25 January 2013, the gap has been filled by using the data from the SSMIS. The SSMIS-based maps have lower resolution, but for compatibility reasons the University of Bremen provides them at the same grid spacing as the AMSR–E products.

Sea-ice drift data are monthly averages of Polar Pathfinder Daily 25 km EASE–Grid Sea Ice Motion Vectors, Version 2, provided by the National Snow and Ice Data Centre from 1 January 2006 to 8 April 2012. They are derived from a wide variety of sensors, for example, AMSR-E and SSMIS, and are available at a spatial resolution of 25 km × 25 km (Tschudi et al. 2016).

The study by Stammerjohn et al. (2015) shows that the length of the ice season, that is, the time elapsed between the days of first sea-ice advance and retreat, has decreased in the Amundsen Sea recent decades. Yet, the ice season duration is still over 300 days in the ASE and about 250 days in the region off the continental shelf. The ASE was never completely ice-free during the study period (Fig. 4).

Iceberg calving estimation

Iceberg calving into the embayment was estimated using the method described by Liu et al. (2015). The images were first aligned using feature tracking. The calved area (i.e., the parts that drifted away, leaving open water between the ice shelf and the iceberg) was then calculated by digitizing the difference between the aligned images (Fig. 5). This procedure removes the effect of an advancing ice front and extracts only the actual calved area. The analysed images (four to five per year to cover the whole ASE) were acquired in February/March, which were the months containing the largest number of images for the region.

The calved area was manually digitized, similar to methods described by Moon & Joughin (2008), Schild & Hamilton (2013) and Liu et al. (2015). An automated method (e.g., Seale et al. 2011) would potentially be quicker, but manual digitalization is usually more accurate, and is still time efficient considering that the data set is small. The pre-processing steps of ASAR data in this study were as those carried out by Mazur et al. (2017) so the errors resulting from resolution limitation should be comparable, that is, the error of area estimation was between 1 and 10%, which was confirmed when comparing the obtained calving rates to those found from Landsat images (with 30 m resolution).

In the present study, iceberg calving was calculated from the actual area loss every year (see also, e.g., Liu et al. 2015). Another method commonly used is to assume a stationary ice shelf front and obtain the iceberg calving from the ice velocity near the front (Depoorter et al. 2013; Rignot et al. 2013). Both methods require information

Citation: *Polar Research* 2019, *38*, 3313, http://dx.doi.org/10.33265/polar.v38.3313

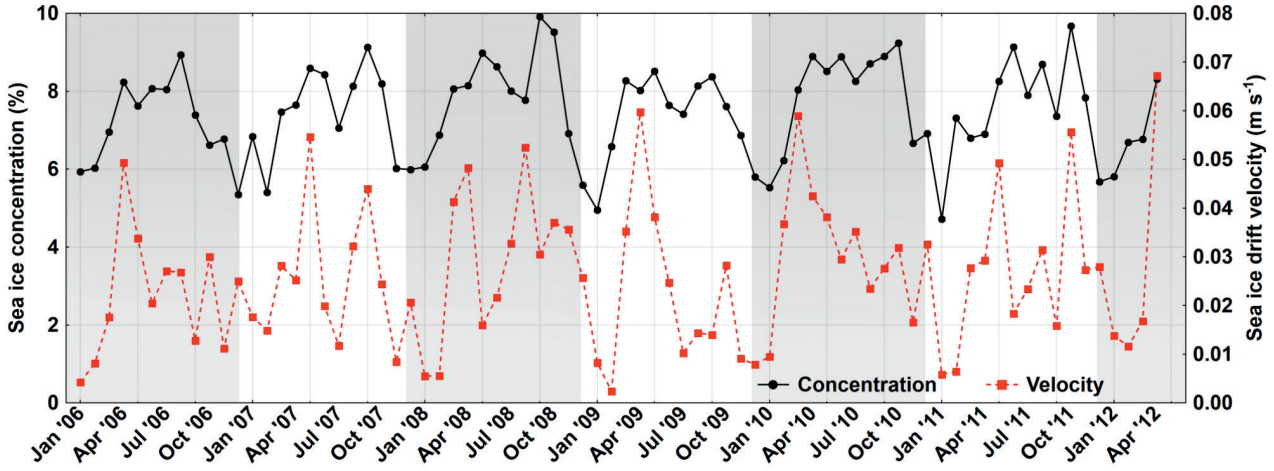

Fig. 4 Monthly AMSR-E (1 January 2006–4 October 2011) and SSMIS (5 October 2011–8 April 2012) mean sea-ice concentration (Spreen et al. 2008) and monthly average sea-ice velocities (Polar Pathfinder Daily 25 km EASE–Grid Sea Ice Motion Vectors [Tschudi et al. 2016]) in the ASE between 1 January 2006 and 8 April 2012. Grey rectangles separate 12-month periods starting on 1 December and ending the following calendar year on 30 November.

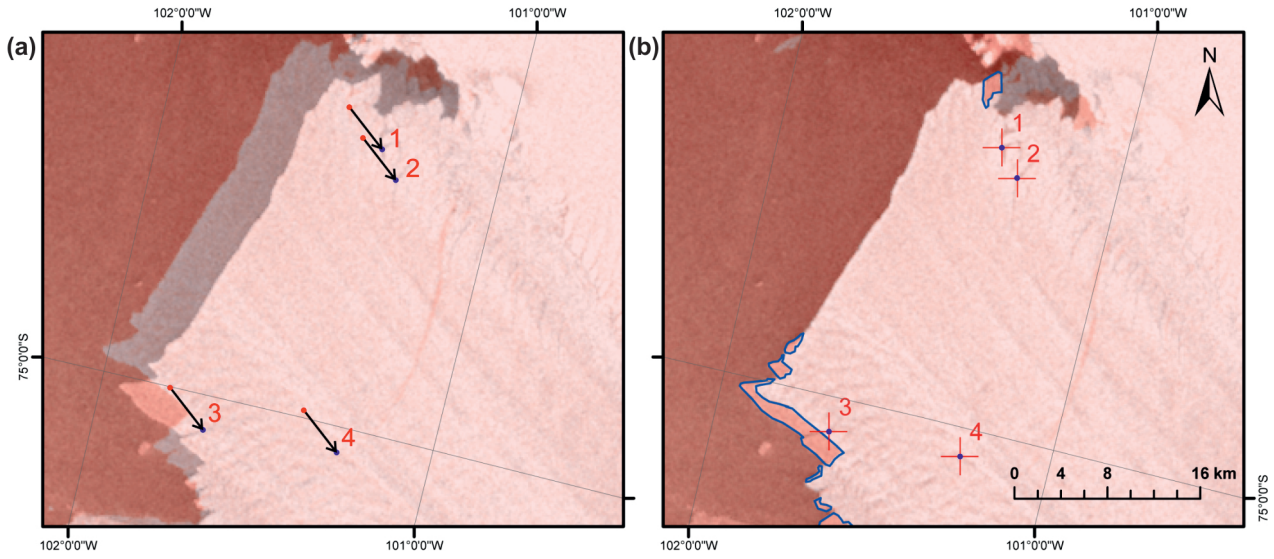

Fig. 5 An example of a detected calved area of the Pine Island Ice Shelf in 2011. ASAR images acquired on 8 February 2011 (grey image below) and 10 February 2012 (transparent red image) area shown (a) on their respective geographical positions and (b) aligned. The points and arrows indicate the features the alignment was based on and the blue lines indicate the digitized area.

about ice thickness and density to get ice mass loss, which is then calculated as the product of the area loss, the mean ice equivalent thickness at the shelf front (Fig. 5) and the ice density. Here we used an ice density of 917 kg m^{-3}. The actual ice thickness of ice shelves is a combination of marine ice and a firn layer. An average ice density is 917 kg m^{-3}; however, the firn layer and other impurities typically lower this value. The ice equivalent thickness presented by Liu et al. (2015), and also used here, is a reduced total thickness, that is, the thickness that the ice shelf would have assuming an average ice density 917 kg m^{-3} for all the ice.

Iceberg classification and characteristics

Icebergs were identified from the calibrated images using the method described by Mazur et al. (2017), an object-based image interpretation with segmentation and classification carried out on different scale levels. They were distinguished based on brightness, contrast and shape qualities using the same thresholds as Mazur et al. (2017) used. The main advantage of this method is that it enables identification of smaller icebergs and enables identification during more difficult conditions. A disadvantage is that over- or underestimates of the numbers can occur as a result of over- or undersegmentation, and that levels of several parameters according to typical scale, backscatter properties, shape and so on have to be set. An example of a classification result is shown in Fig. 6. For more details and specific values for the various parameters, see Mazur et al. (2017).

The detection errors were calculated based on comparison of manually classified icebergs with the result of an automatic classification in different areas and seasons (Mazur et al. 2017). The detection rate was 96.2%, corresponding to 93.2% of the iceberg area. The rate of errors in the form of "false alarms" and "misses" were 3.9 and 3.8%, respectively. However, icebergs smaller than 0.3 km^2 could not be efficiently detected and analysed because of the resolution limitation (Mazur et al. 2017). Nevertheless, a small portion of icebergs less than 0.3 km^2 (around 10%) was detected. We decided not to remove them, so they were kept in the analyses.

In conditions above freezing, icebergs might have melt water on their surface which make them less visible on radar images (Willis et al. 1996; Williams et al. 1999; Wesche & Dierking 2012). For this reason, all the images from December and January for all years were manually examined and those with suspected melt water (between 1 and 20 images each year) were deleted from the analysis (Table 1).

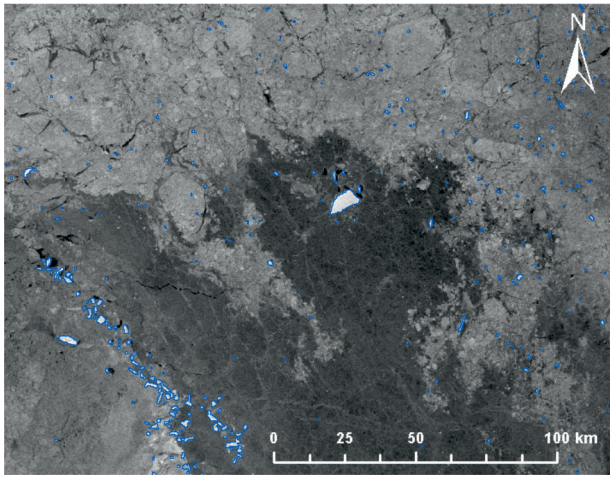

Fig. 6 Outlines of icebergs according to the object-based iceberg classification algorithm, applied to ASAR image taken on 8 July 2011.

The ASAR images were captured somewhat irregularly in space and time. Certain regions have much better coverage than other regions and the coverage varies in time. The data coverage for the whole study period and in different years is presented in Fig. 7.

To quantify length, projected surface area of icebergs, abundance and so on, the parameters are presented in relation to the coverage in a gridded field as basis. The probability of finding an iceberg is equal to the number of times an iceberg was identified in a grid cell (150 m × 150 m), divided by the number of images that had coverage of that cell (Mazur et al. 2017). The probability of finding an iceberg of a certain size in a grid cell is equal to the number of times such an iceberg was identified, divided by the total number of images available for that cell. Total iceberg number and surface area were obtained by studying larger grid cells (15 km × 15 km) and adding up all the average values for the grid cells. Length and size distribution of the icebergs was calculated by dividing the number of icebergs of a certain property in a grid cell by the total number of icebergs in that cell. The resulting histograms show the averaged length and size distributions in all grid cells.

Icebergs are classified based on their size and shape. There are two classification systems in use: the International Ice Patrol and the WMO systems (Willis et al. 1996). With the available resolution all icebergs detected within this work should be classified as very large. In this study, to differentiate between different iceberg sizes, we classify them into small (<10 km^2), medium (10–25 km^2) and large (>25 km^2). Icebergs longer than 10 nautical miles (18.5 km), which are also tracked by NIC, are called giant herein.

The area at the mouth of the Crosson Ice Shelf and Thwaites Ice Tongue (Fig. 1, upper left subset) always has a large number of grounded icebergs surrounded by a mixture of small, clustered icebergs frozen within sea ice, only unreliably detectable with available resolution. This area, plus the area occupied by iceberg B22A (approximately 3500 km^2 in size and considered as a separate ice island), was excluded from the present analysis. Only icebergs leaving these regions were counted.

Iceberg tracking

In addition, 67 icebergs, which were distinguishable on consequent images, were manually selected and their positions were tracked between 1 January 2006 and 8

Citation: *Polar Research* 2019, *38*, 3313, http://dx.doi.org/10.33265/polar.v38.3313

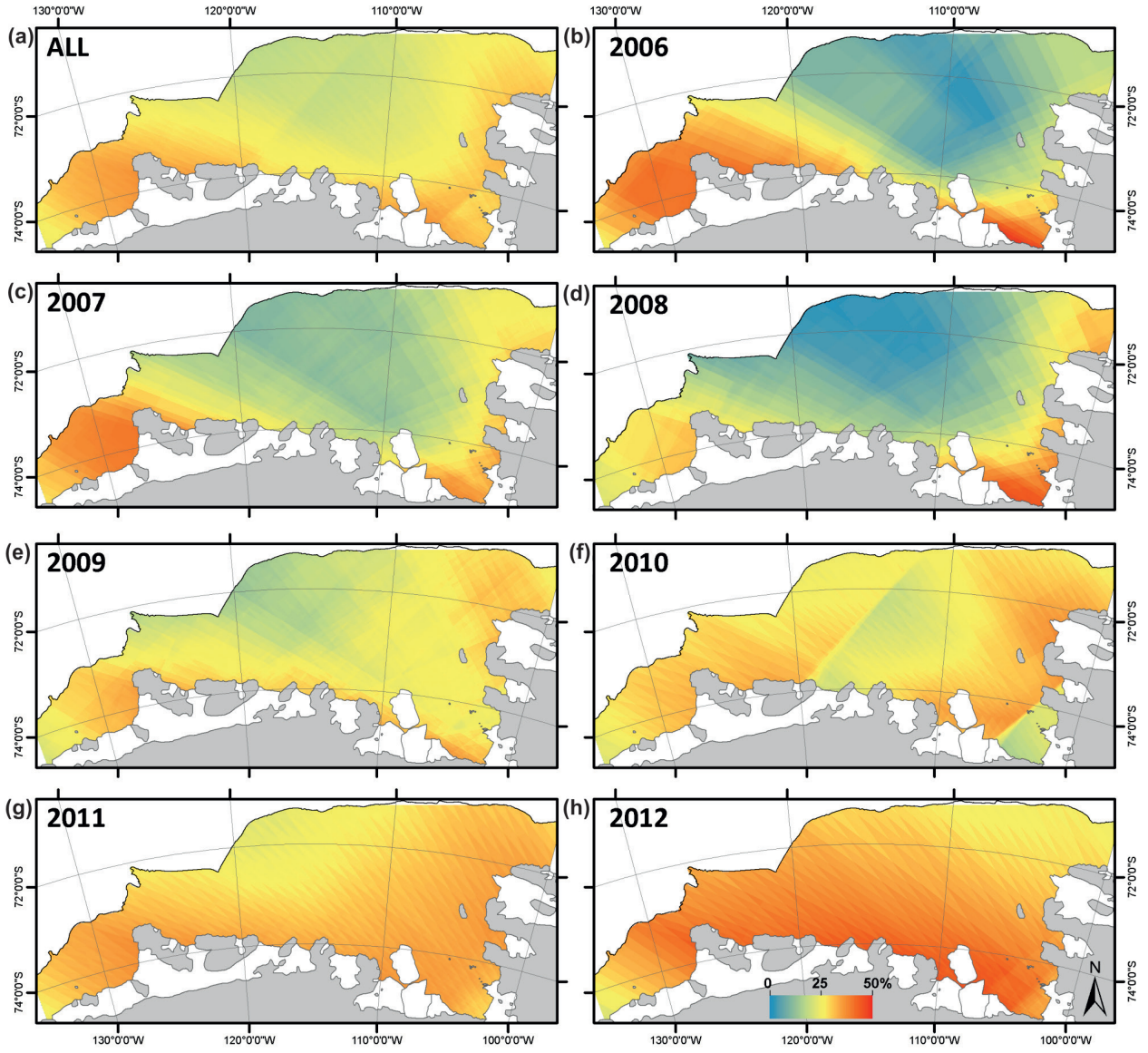

Fig. 7 ASAR Wide Swath Mode data coverage for: (a) all images, images taken in (b) 2006, (c) 2007, (d) 2008, (e) 2009, (f) 2010, (g) 2011 and (h) 2012, in the ASE between 1 January 2006 and 8 April 2012.

April 2012. Based on the number of days those icebergs were present in the Amundsen Sea during the analysed period, their residence time in the ASE was calculated. The iceberg drift speed was calculated based on the Euclidean distance between the central positions of an iceberg detected on consecutive ASAR images with known time interval. The iceberg average drift speed was estimated by dividing the total distance by the total elapsed time, similar to Collares et al. (2018) and Gladstone & Bigg (2002). If iceberg velocity was less than 0.005 m s^{-1}, the iceberg was considered grounded.

Iceberg mass estimation

The measured variable in this study is the projected surface area of the iceberg without any information about its three-dimensional shape. According to the WMO (2015), icebergs can be divided into tabular, domed, sloping or pinnacled shapes, but the majority of the icebergs in the Southern Ocean are classified as weathered, which means that as a result of melting and erosion processes, no regular shape can be assigned to them (Romanov et al. 2012). Considering that the largest icebergs are the tabular ones

and that they constitute 33% of the icebergs present south of 70° in the Western Hemisphere (Romanov et al. 2012), it is assumed here that the icebergs have the form of cuboids for the ice mass calculation purposes.

Although iceberg thickness can be determined from space by using altimeter data (Jansen et al. 2007; Li et al. 2018), it cannot be measured with SAR data. According to Bigg et al. (1997), Gladstone et al. (2001) and Romanov et al. (2012), there is a relationship between the iceberg length and its thickness/freeboard. Romanov et al. (2012) observed the ratio 4:1 between length and freeboard for weathered icebergs and the ratio 9–10:1 for the tabular ones. Both Bigg et al. (1997) and Gladstone et al. (2001) assumed variable thicknesses for icebergs with length up to 500 m and constant values (250 and 360 m, respectively) for the longer ones. Wesche & Dierking (2015), who analysed icebergs longer than 753 m, also assumed 360 m as an average thickness (for comparison purposes, they also presented the results assuming a mean iceberg thickness of 250 m). Silva et al. (2006) also estimated the total iceberg mass assuming an iceberg thickness of 250 m. Considering the fact that most icebergs that could be detected in this study were longer than 500 m, the mean thickness of the icebergs in the ASE was assumed to be 250 m, consistent with Gladstone et al. (2001), Silva et al. (2006), Tournadre et al. (2012) and Tournadre et al. (2015). However, the assumption of fixed iceberg thickness is very simplified.

Similar to ice shelves, the density of icebergs is not constant and a firn layer makes it lower than the density of pure ice. To estimate the ice mass that was present in icebergs, Silva et al. (2006) assumed a mean ice density of 850 kg m^{-3}, Wesche & Dierking (2015) assumed 822 kg m^{-3} and Tournadre et al. (2015) used the value 890 kg m^{-3}. As the study of Wesche & Dierking (2015) is the only work covering the ASE, we also calculated iceberg mass based on the density 822 kg m^{-3} for better comparability.

Results

Figure 8 shows the annual calving rate into the ASE during the six years of study. The average was 620 km^2 yr^{-1} with standard deviation ± 352 km^2 yr^{-1} (177.9 ± 117 Gt yr^{-1}), and there was a significant increase in 2007 caused by calving of the giant iceberg B27 (with an area of 600 km^2) from Pine Island Glacier. Excluding B27 from calculations, the standard deviation of iceberg calving is instead 186 km^2 yr^{-1} (51 Gt yr^{-1}). Contributions from individual ice shelves to the total iceberg calving is shown in Fig. 9. Thwaites, Pine Island and Western Getz Ice Shelf had the highest calving rates: 161.7, 172.2 and 138.7 km^2 yr^{-1}, respectively.

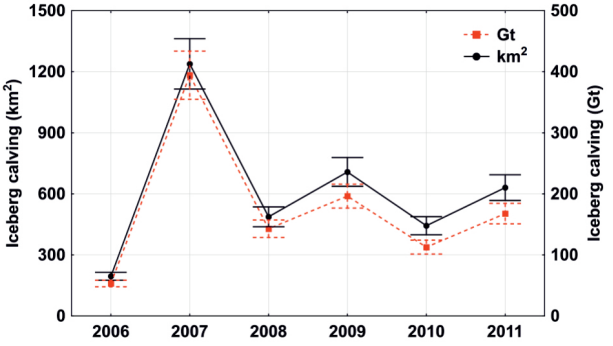

Fig. 8 Annual iceberg calving (black) in km^2 and (red) in Gt in the ASE (2006–2011). Error bars are uncertainties based on the average relative size error estimates according to Mazur et al. (2017).

There were on average 1370 ± 50 icebergs in the ASE, with a combined surface area of 1432.9–1731.2 km^2 (based on the error estimates by Mazur et al. 2017) during the study period. Assuming an average thickness of 250 m and an average density of 822 kg m^{-3}, the average iceberg mass in the ASE during the study period was 316 Gt. Figure 10 shows the average size distribution of these icebergs. Nearly all of them were small (<10 km^2) or medium sized (10–25 km^2). Icebergs smaller than 2 km^2 accounted for almost 90% of the iceberg population but only about 52% of the area, while icebergs larger than 10 km^2 constituted less than 1% of the population by count but up to 16% of the surface area.

Figure 11 shows the variation of iceberg count and the combined surface area for different sizes of icebergs over the study period. The maximum total surface area of 2777.2 km^2 was reached in 2008 after which it decreased gradually to 1368.3 km^2 in 2011, while the number of icebergs had a minimum value in 2009 after which it increased again. While the surface area of small- and medium-sized icebergs remains relatively constant—indicating that export out of the ASE, deterioration/melting and calving are in approximate balance for those bergs—the observed changes in total iceberg area are caused mainly by the largest size class and can be traced back to two giant icebergs: in November 2007, iceberg B27 (around 600 km^2 in size) calved in Pine Island Bay. This iceberg together with iceberg B21 (around 250 km^2 calved in 2001) left the ASE in 2011.

Figure 11 also shows the observed changes of the different size categories. The increase in icebergs >25 km^2 in 2008 (visible in both number and surface area) was followed by an increase in icebergs of small- and medium-sized class in 2009 and in 2010 (Fig. 11). The reason for this is iceberg B27 that calved in November 2007 and then disintegrated into smaller pieces (Fig. 12). Overall,

Citation: *Polar Research* 2019, *38*, 3313, http://dx.doi.org/10.33265/polar.v38.3313

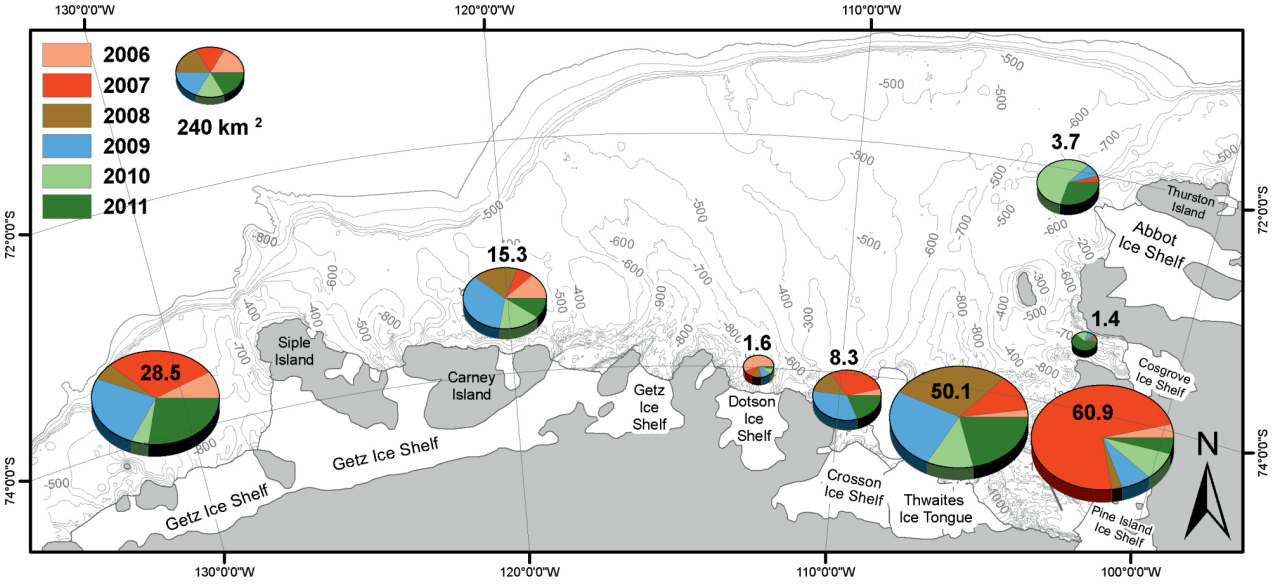

Fig. 9 Iceberg calving from different ice shelves in the ASE during 2006–2011. The pie charts show the annual iceberg calving from indicated ice shelves in km^2. The numbers are values in Gt. Thin lines indicate bathymetry according to IBCSO database (Arndt et al. 2013).

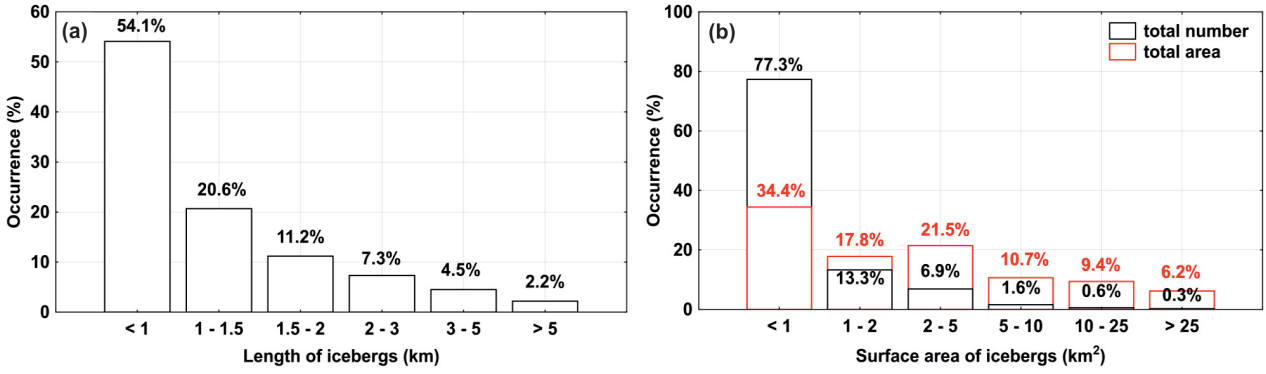

Fig. 10 Average (a) length and (b) percentage of the total number of icebergs (black) and their contribution to the total surface area (red) in the Amundsen Sea between 1 January 2006 and 8 April 2012.

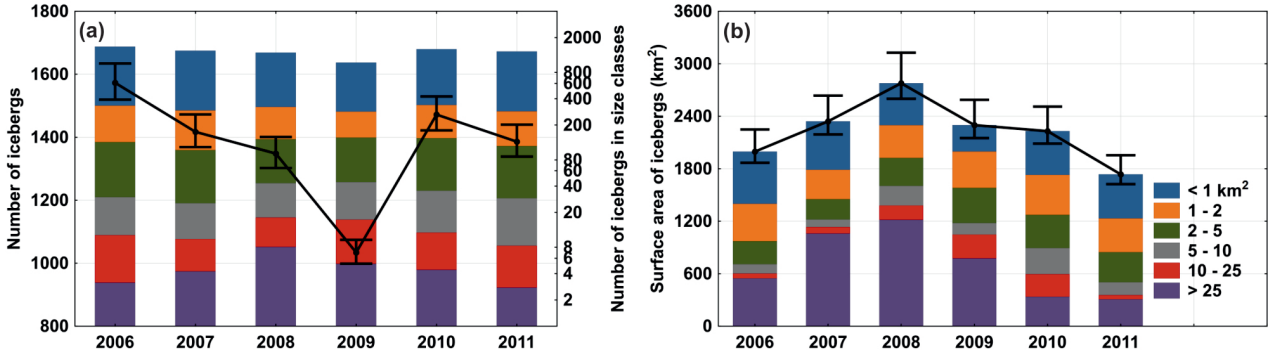

Fig. 11 Annual average (a) number of icebergs (right axis) and (b) surface area of icebergs for different size classes (according to colours). Black solid line shows the total (a) number of icebergs (left axis) and (b) surface area of icebergs in the ASE. Error bars indicate rate of false alarms and misses (Mazur et al. 2017).

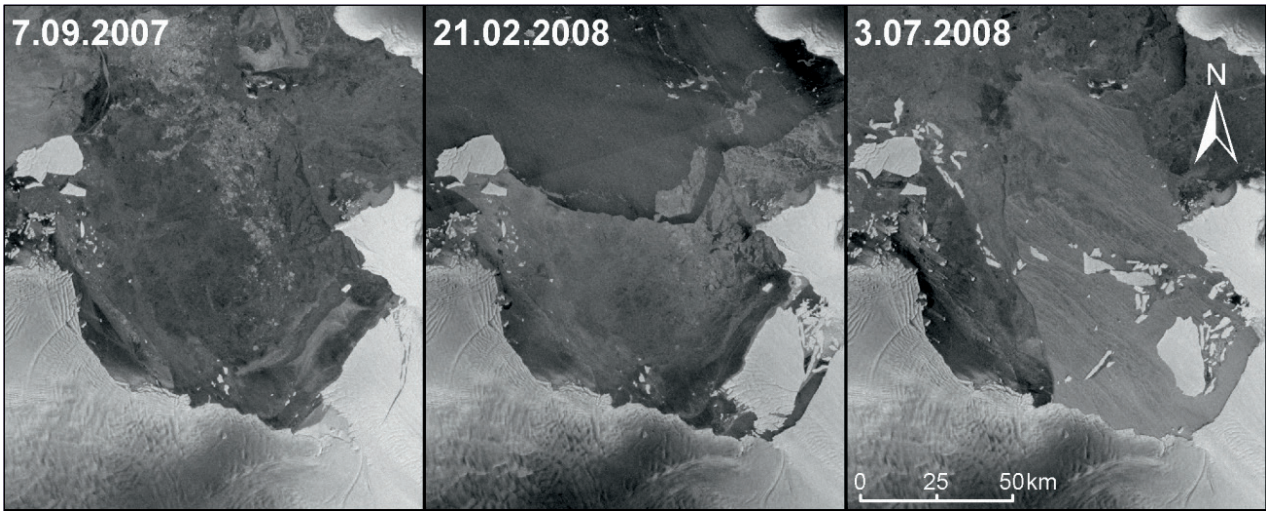

Fig. 12 A sequence of ASAR images taken on 7 September 2007, 21 February 2008 and 3 July 2008 showing the calving and disintegration of the B27 iceberg in the Pine Island Bay.

the values at the start of the study periods are similar to those at the end. There is also no clear variation of small- and medium-sized icebergs except for the decrease in 2009 for icebergs smaller than 2 km^2.

Icebergs can either drift or get stranded on topographic features. Figure 13 shows the probability of finding icebergs of various size classes in the ASE. Icebergs of all sizes accumulate on shallow banks and ridges. In Pine Island Bay, there is quite a high probability (up to 30%) of finding large icebergs, and it is highest on pathways along the deeper parts leading westwards in the ASE. The average observation time for the icebergs was 681 days and it ranged between 39 and 2265 days. The number of observations per iceberg was on average 180 and ranged between 16 and 631. Figure14 shows trajectories of 67 tracked icebergs, grouped into four classes according to their origin and the path they follow. Their average drift speed was 0.027 ± 0.044 m s^{-1} or—disregarding icebergs stranded or stuck in fast sea ice—0.049 ± 0.046 m s^{-1}. Icebergs originating from the Crosson, Thwaites and Getz ice shelves that follow the westward coastal current (Kim et al. 2016) are shown in Fig. 14a. These icebergs have the smallest spatial spread and the lowest average velocity (0.04 ± 0.04 m s^{-1}). Icebergs calved from eastern Thwaites and Pine Island (Fig. 14b) are the largest group with an average velocity 0.05 ± 0.05 m s^{-1}. They first move towards northwest, following the bathymetry along the edge of iceberg B22A and then veer westward after crossing the ridge separating Pine Island Trough from Dotson Trough. Some of these take a more southerly route, while others cross the shelf break to the north. Groups 3 and 4 include icebergs that originate from the Abbot Ice Shelf or are of external eastern origin (the Bellingshausen Sea). Part of these traverses the shelf following a northern route (Fig. 14c) or deviates south (Fig. 14d) along the coast, crossing the shallow area around Burke Island. Both groups include the fastest icebergs with average velocities 0.07 ± 0.06 m s^{-1} and 0.06 ± 0.05 m s^{-1}, respectively.

The average drift velocity of the icebergs varied over the year, reaching maximum in autumn/early winter and middle spring, and minimum in summer and winter (Fig. 15). Figure 16 shows positions of the tracked icebergs for different size classes, together with their residence time in the ASE. The largest icebergs originate in Pine Island Bay and the smaller ones are most abundant in the region north of this bay. The smallest icebergs usually do not reside in the ASE longer than one to two year, while the largest can remain in the basin for six years and more, or get stranded for even longer periods (Fig. 16).

Figure 16 illustrates the two main mechanisms controlling the residence time of icebergs in the ASE: the bathymetry and sea ice. The icebergs that get stranded have a significantly extended residence time in the basin. For example, it took approximately five years until iceberg B27 left the area, and for iceberg B21 it took nine years (based on our observations and NIC data). The presence of sea ice and its drift speed appear to affect the residence time of the non-stranded icebergs in the northern parts, as exemplified by the coinciding drift speeds of icebergs and sea ice (Fig. 15) and the circling motion of the drifting ice bergs in the northeast corner (Fig. 14). The icebergs that float normally leave the area in only a couple of months (Fig. 16).

Citation: *Polar Research* 2019, *38*, 3313, http://dx.doi.org/10.33265/polar.v38.3313

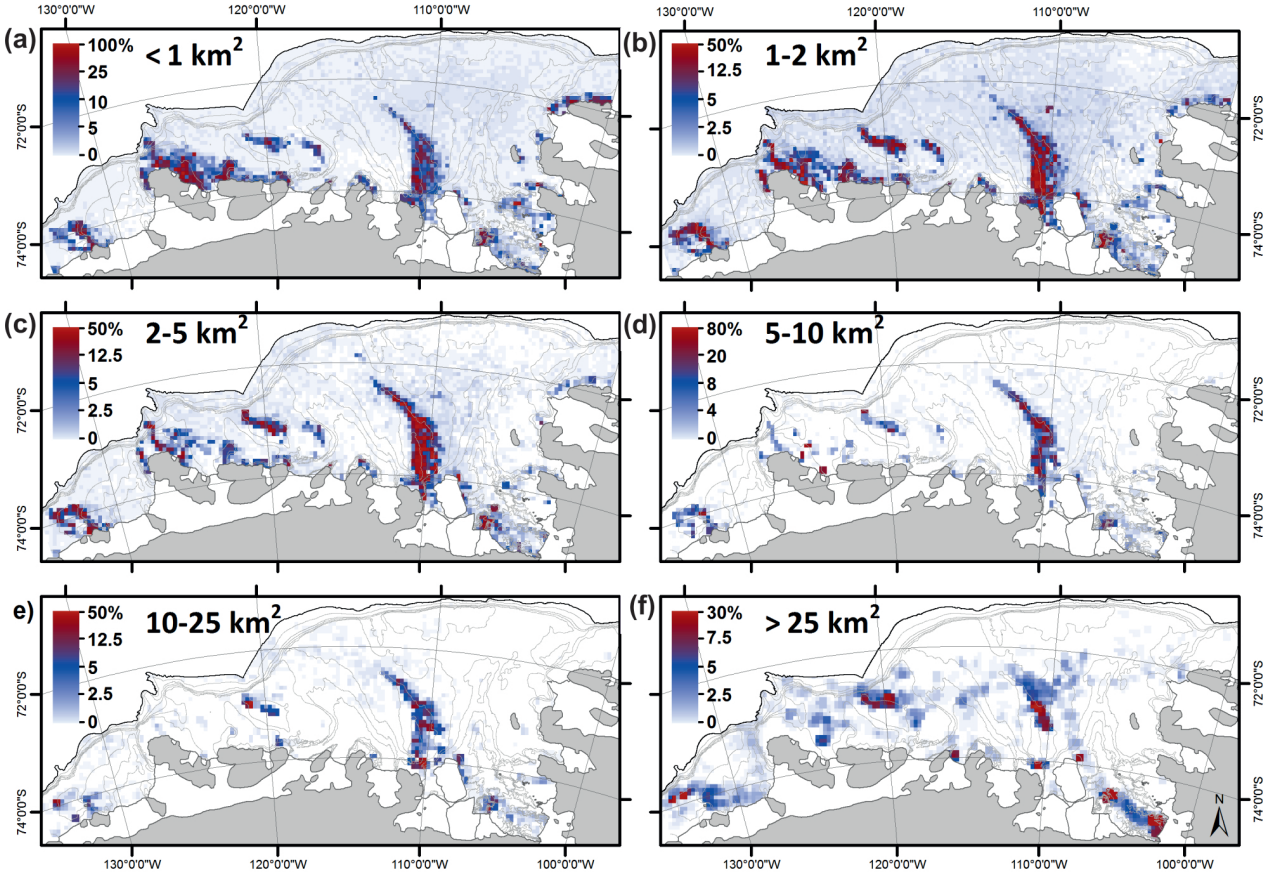

Fig. 13 Probability of finding at least one iceberg of the given size class in a 7.5 km × 7.5 km grid cell: (a) <1 km^2, (b) 1–2 km^2, (c) 2–5 km^2, (d) 5–10 km^2, (e) 10–25 km^2 and (f) >25 km^2, between 1 January 2006 and 8 April 2012. Thin lines indicate bathymetry according to IBCSO database (Arndt et al. 2013).

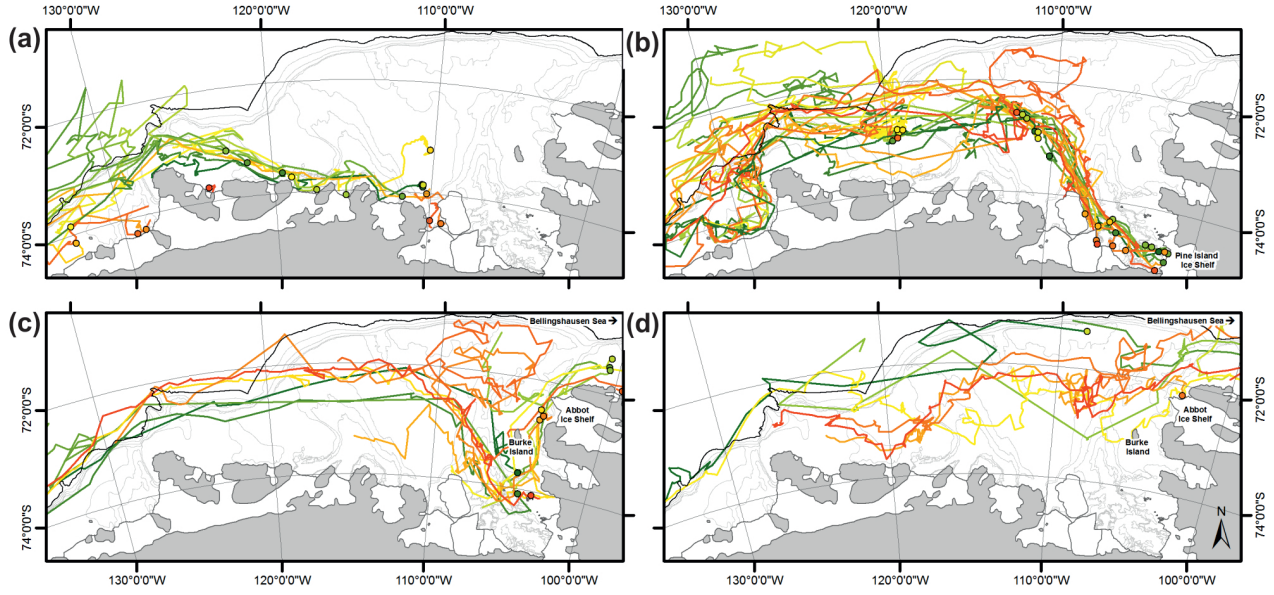

Fig. 14 Iceberg trajectories in different classes: (a) coastal current group, (b) Pine Island group, (c) Bellingshausen/Abbot group which never goes south of Burke Island, (d) Bellingshausen/Abbot South group in the ASE between 1 January 2006 and 8 April 2012. Colours indicate different iceberg trajectories and dots indicate the positions where icebergs started being tracked. Thin lines indicate bathymetry according to IBCSO database (Arndt et al. 2013).

Figure 17 shows the residence time of each iceberg versus its size, based on the trajectories shown in Fig. 16. Although there is no strong correlation between residence time and size, the longest residence times appear to be mostly experienced by icebergs larger than 100 km^2. Most icebergs remain in the area up to three years and almost half for about one year (Fig. 17). The red circle indicates icebergs that were present/grounded in the area at the start of the study and remained present/grounded at the end. Hence, they could have a much larger residence time than indicated in Fig. 17. Of the remaining icebergs, about 15% were present at the start of the study and might also have stayed longer in the area, although the tracking always started in the vicinity of ice shelves. The tracked icebergs all left the area before the end of the study (except the ones circled in Fig. 17).

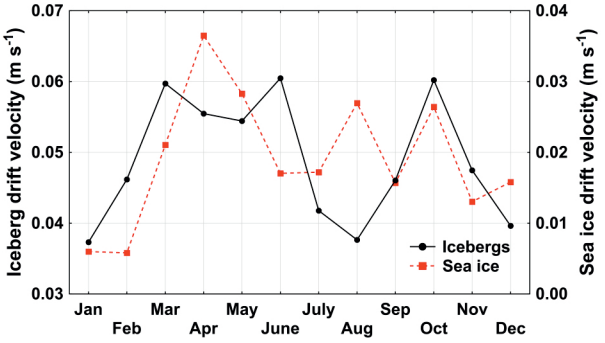

Fig. 15 Mean drift velocities of (black) icebergs and (red) sea ice from Polar Pathfinder Daily 25 km EASE-Grid Sea Ice Motion Vectors (Tschudi et al. 2016) in the ASE in different months between 1 January 2006 and 8 April 2012 (to exclude grounded icebergs from the calculations only icebergs with velocities >0.005 m s^{-1} were considered).

Discussion

The average iceberg calving in the ASE as determined in this study (620 km^2 yr^{-1}/177.9 Gt yr^{-1}) is somewhat smaller than that obtained by Depoorter et al. (2013) and Rignot et al. (2013). Liu et al. (2015) got a significantly higher calving rate, 281.5 Gt yr^{-1}. However, that number includes an unrealistically large (and likely erroneous)

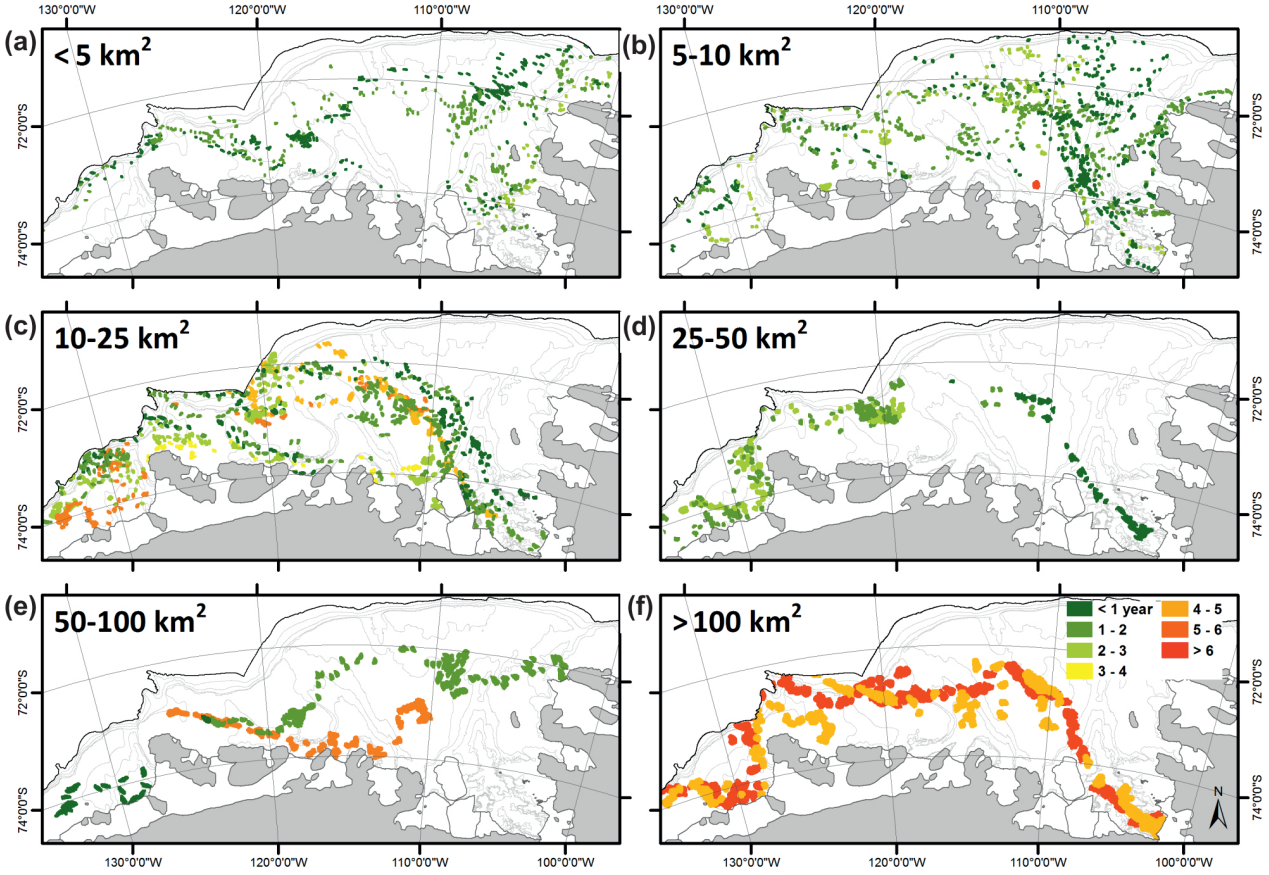

Fig. 16 Residence time of 67 icebergs of different sizes: (a) <5 km^2, (b) 5–10 km^2, (c) 10–25 km^2, (d) 25–50 km^2, (e) 50–100 km^2 and (f) >100 km^2 in the ASE between 1 January 2006 and 8 April 2012. Thin lines indicate bathymetry according to IBCSO database (Arndt et al. 2013).

Citation: *Polar Research* 2019, *38*, 3313, http://dx.doi.org/10.33265/polar.v38.3313

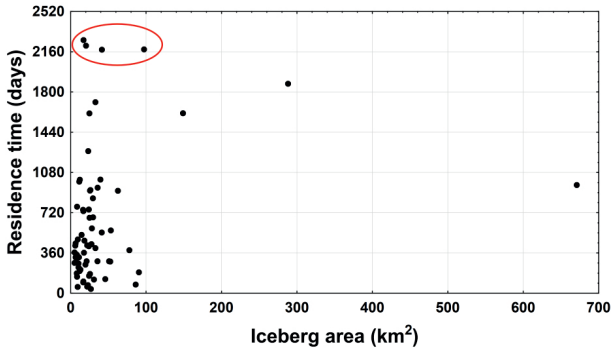

Fig. 17 Residence time of 67 icebergs in relation to their initial surface area in the ASE between 1 January 2006 and 8 April 2012.The red circle indicates icebergs that were present/grounded in the area at the start of the study and remained present/grounded at the end.

annual iceberg calving from Thwaites Ice Tongue: 183 Gt yr^{-1} (corresponding to 600 km^2). In the present study, the calving rate for Thwaites was calculated to 50.1 Gt yr^{-1}, comparable to that obtained by Depoorter et al. (2013) and Rignot et al. (2013). In accordance with those three studies, Thwaites, Pine Island and Western Getz had the highest calving rates in the area over the study period.

The number of icebergs found in the present study is larger than previous estimates for the ASE. According to Wesche & Dierking (2015), there were 497 icebergs in the ASE (with a total surface area of 2189.7 km^2). Their study was limited to icebergs larger than 0.3 km^2. The present study arrives at 2 or 3 times as many icebergs even adjusting for the fact that we include icebergs smaller than 0.3 km^2 (about 10% of the population; see Mazur et al. 2017). One possible explanation for the larger number could be that there were more giant icebergs present, and hence a larger potential source for icebergs in the region. According to the NIC database, two large icebergs were present in the ASE during the 1990s (B10 in 1992 and B11 in 1995), and five between 2001 and 2003 (B21–B25). Considering that most of the calving in 2001–03 occurred from the Crosson and Thwaites ice shelves, it is possible that a portion of the icebergs on the central ridge between 1 January 2006 and 8 April 2012 (Fig. 13) is the grounded, disintegrated remnants of B22–B25 stranded on the ridge. The higher number of icebergs found in the present study compared to that in 1997 (Wesche & Dierking 2015) could therefore be caused by the large iceberg calving events in 2001–03.The fact that there is no clear variation in the number of icebergs between 2006 and 2011 might show that the system then partially adjusted back to a steady state after the heavy calving events of 2001–03, similarly to what was observed in the open-water region of the Pacific sector (Tournadre et al. 2015). This study also exemplifies the process of large icebergs split into smaller ones (Fig. 12). This agrees with the finding of Tournadre et al. (2015) that the main mechanism responsible for disappearance of large icebergs in open water (breakage and disintegration into small icebergs) is also valid in the near-coastal, sea-ice covered region of the ASE.

The ASE iceberg size distribution found in this study agrees qualitatively with previous short-term observations (Romanov et al. 2012; Wesche & Dierking 2015), but is substantially different to the Antarctic-wide open-ocean distribution given by Tournadre et al. (2015), which was based on altimeter data from the sea-ice free region in the Southern Ocean during 2002–2012. The main difference is in the proportion of area covered by icebergs smaller than 10 km^2 (3–4% in Tournadre et al. 2015 compared to 84.4%) and larger than 10 km^2 (96–97% in Tournandre et al. 2015 compared to 15.6%). This can be seen by comparing Fig. 10b to Fig. 6b from Tournadre et al. (2015). An explanation for the differences can be that the data studied by Tournadre et al. (2015) include several large icebergs calved from circumpolar coastal regions of Antarctica that remained for a long time in the Antarctic Circumpolar Current (e.g., pieces of B15 and C19 have resided there for more than 10 years). Such large icebergs form sporadically in the ASE, but represent only a small percentage during the study period. On the contrary, icebergs between 1 and 10 km^2 calve more often and also tend to ground in the ASE, so they can remain in the area for a long time.

Disregarding the giant icebergs, the iceberg surface area in the ASE remained remarkably constant during our study period and on average it is only 20% larger than what was observed in 1997 (Wesche & Dierking 2015). The ice mass stored in icebergs obtained in this study can be compared with the 450 Gt observed in the region in 1997 (Wesche & Dierking 2015), using the same assumptions about thickness and density. However, 193 Gt of the total 450 Gt in the study by Wesche & Dierking was stored in only one iceberg (potentially a piece of iceberg B10). In the present study, large single calving events, such as calving of B27, had a smaller effect on the average because of our longer study period: six year compared to a single observation by Wesche & Dierking (2015). Nevertheless, both estimates are significantly larger than estimates obtained for open water. The entire ice-free part of the ocean around Antarctica had on average 700–800 Gt icebergs between 2006 and 2011, about 40% of which were found in the Pacific Sector (Tournadre et al. 2015). Our results together with the work of Wesche & Dierking (2015) highlight a potential limitation of studies focusing only on open-water areas because large amounts of icebergs will be missed.

In the present study, it was seen that icebergs drift westwards in the ASE (Fig. 14), with the tendency of the largest icebergs to follow the trough systems on the continental shelf (Fig. 16f). The average speed of the icebergs was 0.049 ms^{-1}, which is consistent with the findings of Hamley & Budd (1986) and Aoki (2003), based on observations in East Antarctica, and those obtained in the Weddell Sea (Gladstone & Bigg 2002; Collares et al. 2018), based on trajectories inferred from satellite images. The seasonal variability of drift speed obtained here (Fig. 15) is different from that obtained by Aoki (2003), who observed a maximum iceberg drift speed in autumn and early winter and a minimum in spring. Aoki's results were based on large icebergs (>1200 km^2), which have been shown to depend primarily on ocean currents (see also FitzMaurice et al. 2016; Rackow et al. 2017). However, the icebergs observed in the present study were typically smaller than 2 km^2 and therefore more sensitive to wind forcing and sea-ice drift. According to Wagner et al. (2017), small icebergs (length <200 m) are driven 3 times as strongly by wind than by ocean currents and this ratio becomes less than 10% for icebergs longer than 12 km. Figure 15 shows similarities between iceberg and sea-ice drift velocities, which suggests that icebergs—particularly smaller icebergs—in the Amundsen Sea were also highly influenced by drifting sea ice. The lower drift velocities in winter might be caused by the fact that icebergs are being frozen in sea ice, which was also observed by Marko et al. (1982) and Yulmetov et al. (2016) in the Arctic and Schodlok et al. (2006) in the Weddell Sea.

An approximate estimate of iceberg residence time can be obtained by dividing the total average iceberg area by the average area of iceberg calving. This definition is different from one based on iceberg mass and the mass loss due to calving, which needs information about iceberg thickness and its shape below surface, which can be complex and change during iceberg drift and melt (Moon et al. 2018). The data available show that the average surface area of icebergs in the ASE is 2.5 times larger than the surface area calved into the basin per year. Assuming no melting, this indicates that the average age of the icebergs in the Amundsen Sea is about 2.5 years. This is likely an upper estimate because only a small portion of the icebergs smaller than 0.3 km^2 were counted. Nevertheless, Fig. 17 shows that a majority of the icebergs that were tracked remained in the ASE three years or less, which agrees qualitatively with the surface area-based satellite estimate.

Jacobs et al. (1992), using data from 1979 to 1990, observed a peak in number of giant icebergs in Antarctica in 1986/87, while Long et al. (2002), using data from 1997 to 2001, observed an abrupt increase in 1998. The registered increase in 1998 can be partially explained by the improved observation tools. Tournadre et al. (2015), using altimeter data, and Stuart & Long (2011), using scatterometer data, show peaks in iceberg number between 2002–04 and 2008–2010. Those findings suggest that large calving events in Antarctica occur on timescales of 5–10 years.

The potential decadal periodicity of calving events in the ASE appears to continue with a large number of giant icebergs calved between 2010 and 2015: in 2010 the icebergs B28 and B29 calved from the Crosson or Thwaites ice shelves. As these were grounded before they even started to move, they have not contributed to the analysis in the present study. After the failure of the Envisat satellite on 8 April 2012, several giant icebergs have calved in the region: B30 from Thwaites (in 2012), B31 from Pine Island (in 2013) and another five large icebergs until 2015. The hypothesis of Jacobs et al. (1992)—that large calving events occur regularly—is thus confirmed in the ASE. However, the timescale seems to be 5–10 years and not several decades. When the large icebergs disintegrate, they also affect the population of smaller icebergs, but in between these peaks the population is relatively stable.

Conclusions

In this study, interannual iceberg characteristics and residence time in the ASE have been studied for the first time. The present analysis, combined with previous studies, indicates that there were no significant changes in the amount of icebergs during the study period, and that the iceberg population was produced by a steady stream of calving of small- and medium-sized icebergs from the glaciers draining into the region. Interannual variability was caused mainly by episodic calving of giant icebergs, either into the ASE (such as B27) or into the Bellingshausen Sea and then imported into the ASE after break-up into smaller icebergs. The observed peak in 2008–2010 was caused by the calving of B27 in November 2007 and subsequent break-up into smaller icebergs.

The present study shows, overall, more icebergs in the ASE than were detected in 1997 by Wesche & Dierking (2015): 1370 ± 50 compared to 497. There were also more icebergs residing on topographic ridges, particularly the central ridge area at the mouth of the Crosson and Thwaites ice shelves, compared to the 1997 observations. The surface area in 2011 was smaller than in 2006, but on average about 20% larger than in 1997 (Wesche & Dierking 2015). Our size distributions were similar, with most icebergs being smaller than 1 km^2. However, the area covered by differently sized icebergs was substantially different to the open-ocean size distribution found by

Citation: *Polar Research* 2019, *38*, 3313, http://dx.doi.org/10.33265/polar.v38.3313

Tournadre et al. (2015), in which large- or medium-sized icebergs accounted for most of the area.

The average iceberg surface area during the study period was 1537.5 km^2, about 2.5 times larger than the average annual calved area (620 km^2), giving an approximate estimate of 2.5 years for the average age of the icebergs in the ASE. This coincides with residence time calculations based on drift speed, even though large icebergs might get stranded and remain in the area for a decade or more.

Acknowledgements

The authors acknowledge the Academic Computer Centre in Gdańsk (CI TASK) for the MATLAB license. ASAR images were provided by the European Space Agency for the Cat-1 project C1P.5417. They would also like to thank Christopher Readinger from the US National/NIC for providing the NIC iceberg database.

Disclosure statement

The authors report no conflicts of interest.

Funding

This work was supported by the Polish National Science Centre research grant no. 2016/20/T/ST10/00498 (for the project Detection, Characterization and Effects of Icebergs in the Amundsen Sea, Antarctica) and was also part of the research work at University of Gothenburg, thanks to a Swedish Institute scholarship.

References

Aoki S. 2003. Seasonal and spatial variations of iceberg drift off Dronning Maud Land, Antarctica, detected by satellite scatterometers. *Journal of Oceanography 59*, 629–635, http://dx.doi.org/10.1023/B:JOCE.0000009592.45617.dd.

Arndt J.E., Schenke H.W., Jakobsson M., Nitsche F.O., Buys G., Goleby B., Rebesco M., Bohoyo F., Hong J., Black J., Greku R., Udintsev G., Barrios F., Reynoso-Peralta W., Taisei M. & Wigley R. 2013. The International Bathymetric Chart of the Southern Ocean (IBCSO) Version 1.0—a new bathymetric compilation covering circum-Antarctic waters. *Geophysical Research Letters 40*, 3111–3117, http://dx.doi.org/10.1002/grl.50413.

Bamber J.L., Riva R.E.M., Vermeersen B.L.A. & LeBrocq A.M. 2009. Reassessmentof the potential sea-level rise from a collapse of the West Antarctic Ice Sheet. *Science 324*, 901–903, http://dx.doi.org/10.1126/science.1169335.

Barnes D.K.A. 2017. Iceberg killing fields limit huge potential for benthic blue carbon in Antarctic shallows. *Global Change Biology 23*, 2649–2659, http://dx.doi.org/10.1111/gcb.13523.

Biddle L.C., Kaiser J., Heywood K.J., Thompson A.F. & Jenkins A. 2015. Ocean glider observations of iceberg-enhanced biological production in the northwestern Weddell Sea. *Geophysical Research Letters 42*, 459–465, http://dx.doi.org/10.1002/2014GL062850.

Bigg G., Wadley M., Stevens D. & Johnson J. 1997. Modelling the dynamics and thermodynamics of icebergs. *Cold Regions Science and Technology 26*, 113–135, http://dx.doi.org/10.1016/S0165-232X(97)00012-8.

Bintanja R., van Oldenborgh G.J. & Katsman C.A. 2015. The effect of increased freshwater from Antarctic ice shelves on future trends in Antarctic sea ice. *Annals of Glaciology 56*, 120–126, http://dx.doi.org/10.3189/2015AoG69A001.

Björk G., Söderkvist J., Winsor P., Nikolopoulos A. & Steele M. 2002. Return of the cold halocline layer to the Amundsen Basin of the Arctic Ocean: implications for the sea ice mass balance. *Geophysical Research Letters 29*, article no. 1513, http://dx.doi.org/10.1029/2001GL014157.

Bracegirdle T.J. 2013. Climatology and recent increase of westerly winds over the Amundsen Sea derived from six reanalyses. *International Journal of Climatology 33*, 843–851, http://dx.doi.org/10.1002/joc.3473.

Bracegirdle T.J. & Marshall G.J. 2012. The reliability of Antarctic tropospheric pressure and temperature in the latest global reanalyses. *Journal of Climate 25*, 7138–7146, http://dx.doi.org/10.1175/JCLI-D-11-00685.1.

Collares L.L., Mata M.M., Kerr R., Arigony Neto J. & Barbat M.M. 2018. Iceberg drift and ocean circulation in the northwestern Weddell Sea, Antarctica. *Deep-Sea Research Part II 149*, 10–24, http://dx.doi.org/10.1016/j.dsr2.2018.02.014.

Dee D.P., Uppala S.M., Simmons A.J., Berrisford P., Poli P., Kobayashi S., Andrae U., Balmaseda M.A., Balsamo G., Bauer P., Bechtold P., Beljaars A.C.M., van de Berg L., Bidlot J., Bormann N., Delsol C., Dragani R., Fuentes M., Geer A.J., Haimberger L., Healy S.B., Hersbach H., Hólm E.V., Isaksen L., Kållberg P., Köhler M., Matricardi M., McNally A.P., Monge-Sanz B.M., Morcrette J.-J., Park B.-K., Peubey C., de Rosnay P., Tavolato C., Thépaut J.-N. & Vitart F. 2011. The ERA-Interim reanalysis: configuration and performance of the data assimilation system. *Quarterly Journal of the Royal Meteorological Society 137*, 553–597, http://dx.doi.org/10.1002/qj.828.

Depoorter M.A., Bamber J.L., Griggs J.A., Lenaerts J.T.M., Ligtenberg S.R.M., van den Broeke M.R. & Moholdt G. 2013. Calving fluxes and basal melt rates of Antarctic ice shelves. *Nature 502*, 89–92, http://dx.doi.org/10.1038/nature12567.

ESA 2007. *EnvisatASAR product handbook. Issue 2.2.* Paris: European Space Agency.

ESA 2015. Next ESA SAR toolbox. European Space Agency. Accessed on the internet at https://earth.esa.int/web/nest/home/ on 10 May 2017.

FitzMaurice A., Straneo F., Cenedese C. & Andres M. 2016. Effect of a sheared flow on iceberg motion and melting. *Geophysical Research Letters 43*, 12520–12527, http://dx.doi.org/10.1002/2016GL071602.

Fretwell P., Pritchard H.D., Vaughan D.G., Bamber J.L., Barrand N.E., Bell R., Bianchi C., Bingham R.G., Blankenship D.D., Casassa G., Catania G., Callens D., Conway H., Cook A.J., Corr H.F.J., Damaske D., Damm V., Ferraccioli F., Forsberg R., Fujita S., Gim Y., Gogineni P., Griggs J.A., Hindmarsh R.C.A., Holmlund P., Holt J.W., Jacobel R.W., Jenkins A., Jokat W., Jordan T., King E.C., Kohler J., Krabill W., Riger-Kusk M., Langley K.A., Leitchenkov G., Leuschen C., Luyendyk B.P., Matsuoka K., Mouginot J., Nitsche F.O., Nogi Y., Nost O.A., Popov S.V., Rignot E., Rippin D.M., Rivera A., Roberts J., Ross N., Siegert M.J., Smith A.M., Steinhage D., Studinger M., Sun B., Tinto B.K., Welch B.C., Wilson D., Young D.A., Xiangbin C. & Zirizzotti A. 2013. Bedmap2: improved ice bed, surface and thickness datasets for Antarctica. *The Cryosphere 7*, 375–393, http://dx.doi.org/10.5194/tc-7-375-2013.

Frost V.S., Stiles J.A., Shanmugan K. & Holtzman J. 1982. A model for radar images and its application to adaptive digital filtering of multiplicative noise. *IEEE Transactions on Pattern Analysis and Machine Intelligence PAMI-4*(2), 157–166, http://dx.doi.org/10.1109/TPAMI.1982.4767223.

Gladstone R. & Bigg G. 2002. Satellite tracking of icebergs in the Weddell Sea. *Antarctic Science 14*, 278–287, http://dx.doi.org/10.1017/S0954102002000032.

Gladstone R.M., Bigg G.R. & Nicholls K.W. 2001. Iceberg trajectory modeling and meltwater injection in the Southern Ocean. *Journal of Geophysical Research—Oceans 106*, 19903–19915, http://dx.doi.org/10.1029/2000JC000347.

Hamley T.C. & Budd W.F. 1986. Antarctic iceberg distribution and dissolution. *Journal of Glaciology 32*, 242–251, http://dx.doi.org/10.3189/002214307783258521.

Jacobs S., Helmer H., Doake C., Jenkins A. & Frolich R. 1992. Melting of ice shelves and the mass balance of Antarctica. *Journal of Glaciology 38*, 375–387, http://dx.doi.org/10.3189/S0022143000002252.

Jansen D., Schodlok M. & Rack W. 2007. Basal melting of A-38B: a physical modelconstrained by satellite observations. *Remote Sensing of the Cryosphere 111*, 195–203, http://dx.doi.org/10.1016/j.rse.2007.03.022.

Jongma J.I., Driesschaert E., Fichefet T., Goosse H. & Renssen H. 2009. The effect of dynamic–thermodynamic icebergs on the Southern Ocean climate in a three-dimensional model. *Ocean Modelling 26*, 104–113, http://dx.doi.org/10.1016/j.ocemod.2008.09.007.

Kim T., Ha H., Wåhlin A., Lee S., Kim C., Lee J. & Cho Y. 2017. Is Ekman pumping responsible for the seasonal variation of warm circumpolar deep water in the Amundsen Sea? *Continental Shelf Research 132*, 38–48, https://doi.org/10.1016/j.csr.2016.09.005.

Lancelot C., de Montety A., Goosse H., Becquevort S., Schoemann V., Pasquer B. & Vancoppenolle M. 2009. Spatial distribution of the iron supply to phytoplankton in the Southern Ocean: a model study. *Biogeosciences 6*, 2861–2878, http://dx.doi.org/10.5194/bg-6-2861-2009.

Li T., Shokr M., Liu Y., Cheng X., Li T., Wang F. & Hui F. 2018. Monitoring the tabular icebergs C28A and C28B calved from the Mertz Ice Tongue using radar remote sensing data. *Remote Sensing of Environment 216*, 615–625, http://dx.doi.org/10.1016/j.rse.2018.07.028.

Liu Y., Moore J.C., Cheng X., Gladstone R.M., Bassis J.N., Liu H., Wen J. & Hui F. 2015. Ocean-driven thinning enhances iceberg calving and retreat of Antarctic ice shelves. *Proceedings of the National Academy of Science 112*, 3263–3268, http://dx.doi.org/10.1073/pnas.1415137112.

Long D.G., Ballantyn J. & Bertoia C. 2002. Is the number of Antarctic icebergs really increasing? *Eos, Transactions American Geophysical Union 83*, 469–474, http://dx.doi.org/10.1029/2002EO000330.

Marko J.R., Birch J.R. & Wilson M.A. 1982. A study of long-term satellite-tracked iceberg drifts in Baffin Bay and Davis Strait. *Arctic 35*, 234–240, http://dx.doi.org/10.14430/arctic2322.

Mazur A.K., Wåhlin A.K. & Krężel A. 2017. An object-based SAR image iceberg detection algorithm applied to the Amundsen Sea. *Remote Sensing of Environment 189*, 67–83, http://dx.doi.org/10.1016/j.rse.2016.11.013.

Moon T. & Joughin I. 2008. Changes in ice front position on Greenland's outlet glaciers from 1992 to 2007. *Journal of Geophysical Research—Earth Surface 113*, F02022, http://dx.doi.org/10.1029/2007JF000927.

Moon T., Sutherland D.A, Carroll D., Felikson D., Kehrl L. & Straneo F. 2018. Subsurface iceberg melt key to Greenland fjord freshwater budget. *Nature Geoscience 11*, 49–54, http://dx.doi.org/10.1038/s41561-017-0018-z.

Rackow T., Wesche C., Timmermann R., Hellmer H.H., Juricke S. & Jung T. 2017. A simulation of small to giant Antarctic iceberg evolution: differential impact on climatology estimates. *Journal of Geophysical Research—Oceans 122*, 3170–3190, http://dx.doi.org/10.1002/2016JC012513.

Raiswell R., Benning L., Tranter M. & Tulaczyk S. 2008. Bioavailable iron in the Southern Ocean: the significance of the iceberg conveyor belt. *Geochemical Transactions 9*, article no. 7, http://dx.doi.org/10.1186/1467-4866-9-7.

Rignot E., Jacobs S., Mouginot J. & Scheuchl B. 2013. Ice-shelf melting around Antarctica. *Science 341*, 266–270, http://dx.doi.org/10.1126/science.1235798.

Romanov Y.A., Romanova N.A. & Romanov P. 2012. Shape and size of Antarctic icebergs derived from ship observation data. *Antarctic Science 24*, 77–87, http://dx.doi.org/10.1017/S0954102011000538.

Rosich B. & Meadows P. 2004. *Absolute calibration of ASAR level 1 products generated with PF–ASAR.* Rome: European Space Agency.

Schild K.M. & Hamilton G.S. 2013. Seasonal variations of outlet glacier terminus position in Greenland. *Journal of Glaciology 59*, 759–769, http://dx.doi.org/10.3189/2013JoG12J238.

Schodlok M.P., Hellmer H.H., Rohardt G. & Fahrbach E. 2006. Weddell Sea iceberg drift: five years of observations. *Journal of Geophysical Research—Oceans 111*, C06018, http://dx.doi.org/10.1029/2004JC002661.

Seale A., Christoffersen P., Mugford R.I. & O'Leary M. 2011. Ocean forcing of the Greenland ice sheet: calving fronts and patterns of retreat identified by automatic satellite monitoring of eastern outlet glaciers. *Journal of Geophysical Research—Earth Surface 116*, F03013, http://dx.doi.org/10.1029/2010JF001847.

Silva T.A.M., Bigg G.R. & Nicholls K.W. 2006. Contribution of giant icebergs to the Southern Ocean freshwater flux. *Journal of Geophysical Research—Oceans 111*, C03004, http://dx.doi.org/10.1029/2004JC002843.

Smith K.L., Robison B.H., Helly J.J., Kaufmann R.S., Ruhl H.A., Shaw T.J., Twining B.S. & Vernat M. 2007. Free-drifting icebergs: hot spots of chemical and biological enrichment in the Weddell Sea. *Science 317*, 478–483, http://dx.doi.org/10.1126/science.1142834

Spreen G., Kaleschke L. & Heygster G. 2008. Sea ice remote sensing using AMSR–89-GHz channels. *Journal of Geophysical Research—Oceans 113*, C02S03, http://dx.doi.org/10.1029/2005JC003384.

Stammerjohn S., Maksym T., Massom R.A., Lowry K.E., Arrigo K.R., Yuan X., Raphael M., Randall-Goodwin E., Sherrell R.M. & Yager P.L. 2015. Seasonal sea ice changes in the Amundsen Sea, Antarctica, over the period of 1979–2014. *Elementa: Science of the Antropocene 3*, article no. 000055, http://doi.org/10.12952/journal.elementa.000055.

Stern A.A., Johnson E., Holland D.M., Wagner T.J., Wadhams P., Bates R., Abrahamsen E.P., Nicholls K.W., Crawford A., Gagnon J. & Tremblay J.-E. 2015. Wind-driven upwelling around grounded tabular icebergs. *Journal of Geophysical Research—Oceans 120*, 5820–5835, http://dx.doi.org/10.1002/2015JC010805.

Stuart K. & Long D. 2011. Tracking large tabular icebergs using the Sea

Winds Ku-band microwave scatterometer. *Deep-Sea Research Part II 58*, 1285–1300, http://dx.doi.org/10.1016/j.dsr2.2010.11.004.

Tournadre J., Bouhier N., Girard-Ardhuin F. & Rémy F. 2015. Antarctic icebergs distributions 1992–2014. *Journal of Geophysical Research—Oceans 121*, 327–349, http://dx.doi.org/10.1002/2015JC011178.

Tournadre J., Girard-Ardhuin F. & Legrésy B. 2012. Antarctic icebergs distributions, 2002–2010. *Journal of Geophysical Research—Oceans 117*, C05004, http://dx.doi.org/10.1029/2011JC007441.

Tournadre J., Whitmer K. & Ardhuin F. 2008. Iceberg detection in open water by altimeter waveform analysis. *Journal of Geophysical Research—Oceans 113*, C08040, http://dx.doi.org/10.1029/2007JC004587.

Tschudi M., Fowler C., Maslanik J., Stewart J.S. & Meier W.N. 2016. Polar Pathfinder daily 25 km EASE–grid sea ice motion vectors. Version 3. Boulder, CO: National Snow and Ice Data Center, http://dx.doi.org/10.1029/2007JC004587.

Wagner T.J.W., Dell R W. & Eisenman I. 2017. An analytical model of iceberg drift. *Journal of Physical Oceanography 47*, 1605–1616, http://dx.doi.org/10.1175/JPO-D-16-0262.1.

Wesche C. & Dierking W. 2012. Iceberg signatures and detection in synthetic aperture radar (SAR) images in two test regions of the Weddell Sea, Antarctica. *Journal of Glaciology 58*, 325–339, http://dx.doi.org/10.3189/2012J0G11J020.

Wesche C. & Dierking W. 2015. Near-coastal circum-Antarctic iceberg size distributions determined from synthetic aperture radar images. *Remote Sensing of Environment 156*, 561–569, http://dx.doi.org/10.1016/j.rse.2014.10.025.

Williams R.N., Rees W.G. & Young N.W. 1999. A technique for the identification and analysis of icebergs in synthetic aperture radar images of Antarctica. *International Journal of Remote Sensing 20*, 3183–3199, http://dx.doi.org/10.1080/014311699211697.

Willis C.J., Macklin J.T., Partington K.C., Teleki K.A., Rees W.G. & Williams R.G. 1996. Iceberg detection using ERS–1 synthetic aperture radar. *International Journal of Remote Sensing 17*, 1777–1795, http://dx.doi.org/10.1080/01431169608948739.

WMO 2015. *WMO sea-ice nomenclature. Vol. 1. Terminology and codes. WMO-IOC JCOMM Sea-Ice Regulatory Document no. 259.* Geneva: World Meteorological Organization.

Yulmetov R., Marchenko A. & Løset S. 2016. Iceberg and sea ice drift tracking and analysis off north-east Greenland. *Ocean Engineering 123*, 223–237, http://dx.doi.org/10.1016/j.oceaneng.2016.07.012.